













RESEARCH ARTICLE | SEPTEMBER 11 2023

## Singlet–triplet dephasing in radical pairs in avian cryptochromes leads to time-dependent magnetic field effects

Matthew J. Golesworthy ; Tilo Zollitsch; Jiatae Luo; Dan Selby; Lauren E. Jarocho ; Kevin B. Henbest ; Olivier Paré-Labrosse; Rabea Bartölke ; Jessica Schmidt; Jingjing Xu ; Henrik Mouritsen ; P. J. Hore  ; Christiane R. Timmel  ; Stuart R. Mackenzie  



*J. Chem. Phys.* 159, 105102 (2023)

<https://doi.org/10.1063/5.0166675>



CrossMark

### Articles You May Be Interested In

Anisotropic magnetic field effects in the re-oxidation of cryptochrome in the presence of scavenger radicals

*J. Chem. Phys.* (January 2022)

Spin relaxation of radicals in cryptochrome and its role in avian magnetoreception

*J. Chem. Phys.* (July 2016)

On the optimal relative orientation of radicals in the cryptochrome magnetic compass

*J. Chem. Phys.* (August 2019)

500 kHz or 8.5 GHz?  
And all the ranges in between.

Lock-in Amplifiers for your periodic signal measurements



Find out more



# Singlet–triplet dephasing in radical pairs in avian cryptochromes leads to time-dependent magnetic field effects

Cite as: J. Chem. Phys. 159, 105102 (2023); doi: 10.1063/5.0166675

Submitted: 6 July 2023 • Accepted: 21 August 2023 •

Published Online: 11 September 2023












View Online



Export Citation



CrossMark

Matthew J. Golesworthy,<sup>1</sup>  Tilo Zollitsch,<sup>1</sup> Jiate Luo,<sup>1</sup> Dan Selby,<sup>1</sup> Lauren E. Jarocho,<sup>1,2</sup>   
Kevin B. Henbest,<sup>1</sup>  Olivier Paré-Labrosse,<sup>1</sup> Rabea Bartölke,<sup>3</sup>  Jessica Schmidt,<sup>3</sup> Jingjing Xu,<sup>3</sup>   
Henrik Mouritsen,<sup>3,4</sup>  P. J. Hore,<sup>1,a)</sup>  Christiane R. Timmel,<sup>1,a)</sup>  and Stuart R. Mackenzie<sup>1,a)</sup> 

## AFFILIATIONS

<sup>1</sup> Department of Chemistry, University of Oxford, Oxford, United Kingdom

<sup>2</sup> Department of Chemistry, Furman University, Greenville, South Carolina 29613, USA

<sup>3</sup> AG Neurosensory Sciences/Animal Navigation, Institut für Biologie und Umweltwissenschaften, Carl-von-Ossietzky Universität Oldenburg, Oldenburg, Germany

<sup>4</sup> Research Centre for Neurosensory Sciences, University of Oldenburg, Oldenburg, Germany

<sup>a)</sup> Authors to whom correspondence should be addressed: [peter.hore@chem.ox.ac.uk](mailto:peter.hore@chem.ox.ac.uk); [christiane.timmel@chem.ox.ac.uk](mailto:christiane.timmel@chem.ox.ac.uk); and [stuart.mackenzie@chem.ox.ac.uk](mailto:stuart.mackenzie@chem.ox.ac.uk)

## ABSTRACT

Cryptochrome 4a (Cry4a) has been proposed as the sensor at the heart of the magnetic compass in migratory songbirds. Blue-light excitation of this protein produces magnetically sensitive flavin–tryptophan radical pairs whose properties suggest that Cry4a could indeed be suitable as a magnetoreceptor. Here, we use cavity ring-down spectroscopy to measure magnetic field effects on the kinetics of these radical pairs in modified Cry4a proteins from the migratory European robin and from nonmigratory pigeon and chicken.  $B_{1/2}$ , a parameter that characterizes the magnetic field-dependence of the reactions, was found to be larger than expected on the basis of hyperfine interactions and to increase with the delay between pump and probe laser pulses. Semiclassical spin dynamics simulations show that this behavior is consistent with a singlet–triplet dephasing (STD) relaxation mechanism. Analysis of the experimental data gives dephasing rate constants,  $r_{STD}$ , in the range  $3\text{--}6 \times 10^7 \text{ s}^{-1}$ . A simple “toy” model due to Maeda, Miura, and Arai [Mol. Phys. **104**, 1779–1788 (2006)] is used to shed light on the origin of the time-dependence and the nature of the STD mechanism. Under the conditions of the experiments, STD results in an exponential approach to spin equilibrium at a rate considerably slower than  $r_{STD}$ . We attribute the loss of singlet–triplet coherence to electron hopping between the second and third tryptophans of the electron transfer chain and comment on whether this process could explain differences in the magnetic sensitivity of robin, chicken, and pigeon Cry4a’s.

© 2023 Author(s). All article content, except where otherwise noted, is licensed under a Creative Commons Attribution (CC BY) license (<http://creativecommons.org/licenses/by/4.0/>). <https://doi.org/10.1063/5.0166675>

## I. INTRODUCTION

Although it was established more than 50 years ago that migratory songbirds navigate with the help of a magnetic compass,<sup>1–3</sup> the biophysical mechanism of this extraordinary sense is still largely a mystery.<sup>4–14</sup> The leading hypothesis centers on radical pairs formed photochemically in cryptochrome proteins located in photoreceptor cells in the birds’ retinas.<sup>15–17</sup> Studies of the purified proteins

strongly suggest that, of the six known avian cryptochromes, Cry4a is the most likely to have a magnetoreceptive function<sup>18–23</sup> and that the sensor is a flavin–tryptophan radical pair formed by light-induced electron hopping along a chain of four tryptophan (Trp) residues stretching  $\sim 20$  Å from the flavin adenine dinucleotide (FAD) chromophore in the interior of the protein out to its surface.<sup>22</sup>

Weak magnetic fields can affect the kinetics and product yields of radical pair reactions by altering the extent and timing of the

coherent interconversion of the joint singlet and triplet electronic states of the two radicals.<sup>17</sup> The time required for this is of the order of the electron Larmor period,  $(\gamma_e B/2\pi)^{-1}$ , which is  $\sim 700$  ns in the Earth's magnetic field,  $B \approx 50 \mu\text{T}$  ( $\gamma_e$  is the electron magnetogyric ratio). Therefore, to be a geomagnetic sensor, the radical pair must persist for at least  $\sim 700$  ns and so must the spin coherence.<sup>17</sup> It is easier to imagine how the former could be achieved in practice. Processes that limit the lifetime of a radical pair in cryptochrome include electron transfer between the radicals and changes in their protonation states,<sup>17</sup> which depend on factors such as redox potentials, separations between radicals, and availability of proton donors/acceptors, all of which could have been tuned by evolution to achieve the requisite lifetime.

Spin relaxation is potentially more of a problem. It arises from stochastic molecular motions causing fluctuations in the local magnetic fields experienced by the electrons<sup>24–26</sup> and leads to the loss of spin coherence and spin correlation. With the exception of small organic radicals undergoing rapid (picosecond) rotational diffusion in nonviscous liquids, electron spin relaxation as slow as  $\sim 700$  ns is uncommon and it is unclear how this could be achieved for radicals generated inside a protein in a cellular setting at physiological temperatures ( $\sim 40^\circ\text{C}$ ). Relatively little is known about the rates and mechanisms of spin relaxation of FAD–tryptophan radical pairs in cryptochromes in magnetic fields as weak as  $50 \mu\text{T}$ . Behavioral experiments on Eurasian blackcaps subject to broadband radio frequency electromagnetic noise imply spin equilibration on a  $2\text{--}10 \mu\text{s}$  timescale *in vivo*,<sup>27</sup> while all-atom molecular dynamics simulations of a plant cryptochrome in combination with Redfield relaxation theory suggest relaxation times of the order of  $1 \mu\text{s}$ .<sup>24</sup> Other computational studies of radical pair magnetoreceptors have, explicitly or implicitly, assumed spin relaxation to be negligible on timescales of up to a millisecond or longer. In short, there is a great deal of uncertainty about the potentially calamitous effects spin relaxation could have on the sensitivity of a cryptochrome-based magnetic sensor.

Direct measurements of spin coherence lifetimes in radical pairs are difficult and little progress has been made to date. EPR (electron paramagnetic resonance) spectroscopy in a magnetic field of  $\sim 50 \mu\text{T}$  is technically challenging, especially for short-lived radicals in an environment that resembles the conditions *in vivo* which remain largely unknown (but see Refs. 28 and 29). Although measurements on model systems in magnetic fields approaching  $50 \mu\text{T}$  have been reported,<sup>30,31</sup> it has so far proved difficult to achieve sufficient signal-to-noise to detect  $< 1$  mT magnetic field effects on cryptochromes. An indirect source of information on the spin relaxation of radical pairs in cryptochromes would therefore be welcome. In this report, we exploit the effects of magnetic fields much stronger than  $50 \mu\text{T}$ . Typically, for magnetic fields in the range  $1\text{--}100$  mT, the quantum yields of the products of radical pair reactions have a sigmoidal dependence on the intensity of the applied magnetic field characterized by  $B_{1/2}$ , the field strength at which the reaction yield equals the mean of the yields at zero field and at high field. The measured value of  $B_{1/2}$  for a particular radical pair contains information on its hyperfine interactions, its lifetime, and, importantly in the present context, its spin relaxation.<sup>32–34</sup>

In the study reported here, we measured values of  $B_{1/2}$  for Cry4a proteins from European robin (*Erithacus rubecula*, Er), pigeon (*Columba livia*, Cl), and chicken (*Gallus gallus*, Gg) with the aim of

learning more about the mechanisms and rates of spin relaxation in cryptochrome radical pairs. In particular, we wanted to shed light on the observation that Cry4a from a migratory bird (the robin) appears to be more magnetically sensitive than the Cry4a's from two nonmigratory birds (pigeon and chicken).<sup>22,35</sup> As found previously for ErCry4a,<sup>22</sup> the wild type proteins are less magnetically sensitive *in vitro* than their W369F mutants in which the terminal tryptophan of the Trp-tetrad is replaced by a redox-inactive phenylalanine (an effect attributed to the larger radical–radical separation and hence slower radical recombination in the intact proteins). This has made it difficult to obtain reliable values of  $B_{1/2}$  for the wild type proteins. For all three species, measurements were therefore made on the W369F mutants.

## II. METHODS

### A. Cavity ring-down spectroscopy

The homebuilt cavity ring-down spectrometer employed in these studies has been described previously.<sup>22</sup> Briefly, the sample was contained within a  $160 \mu\text{L}$ , 1 mm optical path-length quartz flow cell (Hellma 165-1-40) with high-quality optical windows. The cell, maintained at  $5^\circ\text{C}$  by flowing a chilled water–glycerol mixture through its cooling jacket, sat centrally within an optical cavity formed by two high reflectivity plano-convex mirrors ( $R > 99.5\%$  across the wavelength range  $400 \text{ nm} < \lambda < 800 \text{ nm}$ , Layertec). Direct 450 nm photoexcitation was performed using the  $300 \mu\text{J}$  pulsed output (8 ns pulse length) of a Sirah Nd:YAG-pumped dye laser, aligned off-axis. The 530 nm probe light was provided by 10 ns,  $4.4 \pm 0.3$  mJ pulses from an optical parametric oscillator (Opotek) and was introduced into the cavity via the front cavity mirror. Light exiting the cavity was detected using a photomultiplier tube and recorded with either a digital storage oscilloscope or a data acquisition card. The decay of the light oscillating in the cavity was fitted to a single exponential to determine the ring-down time,  $\tau$ . The per-pass absorbance  $A$  was then determined from  $\tau$  as  $A = L/[c\tau \ln(10)]$ , in which  $L$  is the cavity length,  $c$  is the speed of light and the  $\ln(10)$  factor converts between common and natural logarithms.<sup>36,37</sup> In practice, the absolute extinction is of limited interest as it is determined not only by the sample but also by losses at the cell windows and mirrors and by scattering. Instead, we recorded a differential measurement of absorbance  $\Delta A$ , which represents the change in absorbance induced by the pump laser as follows:

$$\Delta A(t_d) = A_{hv} - A_0 = \frac{1}{\ln(10)} \frac{L}{c} \left( \frac{1}{\tau} - \frac{1}{\tau_0} \right), \quad (1)$$

where  $A_{hv}$  and  $\tau$  are the per-pass absorbance and ring-down time at a time  $t_d$  after the pump pulse while  $A_0$  and  $\tau_0$  are the same quantities recorded without a pump pulse. The pump–probe delay time,  $t_d$ , was controlled by a digital delay generator controlling the two laser systems.

The sample cell was surrounded by homebuilt Helmholtz coils providing 3 ms, 0–30 mT magnetic field pulses. Ring-down traces, which lasted only a few microseconds, were collected once the magnetic field had stabilized. Magnetic field effects,  $\Delta\Delta A(t_d, B)$ , were recorded by measuring differences in  $\Delta A$  with and without an applied magnetic field,  $B$ :  $\Delta\Delta A(t_d, B) = \Delta A(t_d, B) - \Delta A(t_d, 0)$ . The studies described here focus on variation in the

field-dependence of the magnetic field effect as a function of  $t_d$ . To mitigate long-term cavity drift and/or sample photodegradation, measurements were performed in randomized order of magnetic field strengths and/or pump-probe delays. To minimize photobleaching and photoinduced aggregation, the experiments were typically run at 1 Hz, controlled by laser shutters, with additional extended delays designed to allow re-oxidation of long-lived radicals. In order to accumulate sufficient signal-to-noise, the experiment typically continued until 150 individual measurements had been taken at each field strength or pump-probe delay time.

## B. Protein expression and purification

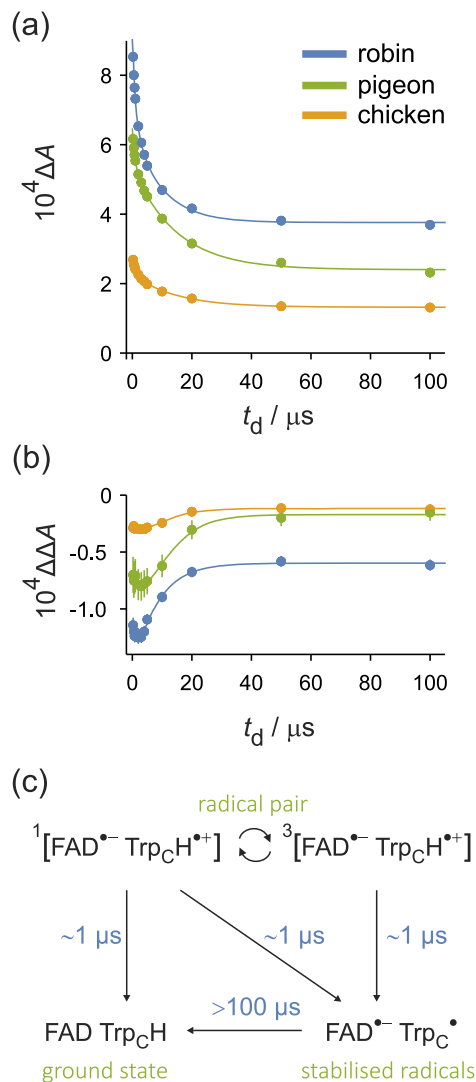
The W369F mutant of *ErCry4a* had been expressed previously.<sup>22</sup> The W369F mutants of *GgCry4a* and *CiCry4a* were newly expressed for this study. All three proteins were cloned, expressed, and purified as described in detail in the work of Xu *et al.*<sup>22</sup> Briefly, proteins were expressed in BL21(DE3) *E. coli* cells in LB media for 22 h and 15 °C in the dark. The optimal IPTG (isopropyl-D-1-thiogalactopyranoside) concentration for induction was 5  $\mu$ M for *ErCry4a* W369F and 10  $\mu$ M for *GgCry4a* and *CiCry4a* W369F mutants. Cells were harvested and lysed as described previously.<sup>22</sup> Protein purification of the cleared lysate was accomplished in two steps: (1) first Ni-NTA chromatography, (2) followed by anion exchange chromatography. Purified proteins were concentrated and snap frozen in liquid nitrogen in a storage buffer containing 20 mM Tris (pH 8.0), 20% glycerol, 10 mM 2-mercaptoethanol, and 110–250 mM NaCl, depending on the isoelectric point of the protein. Primers used for the site-specific mutagenesis of *GgCry4a* W369F and *CiCry4a* W369F are listed in Table S1.

## III. RESULTS

### A. Radical kinetics and magnetic field effects

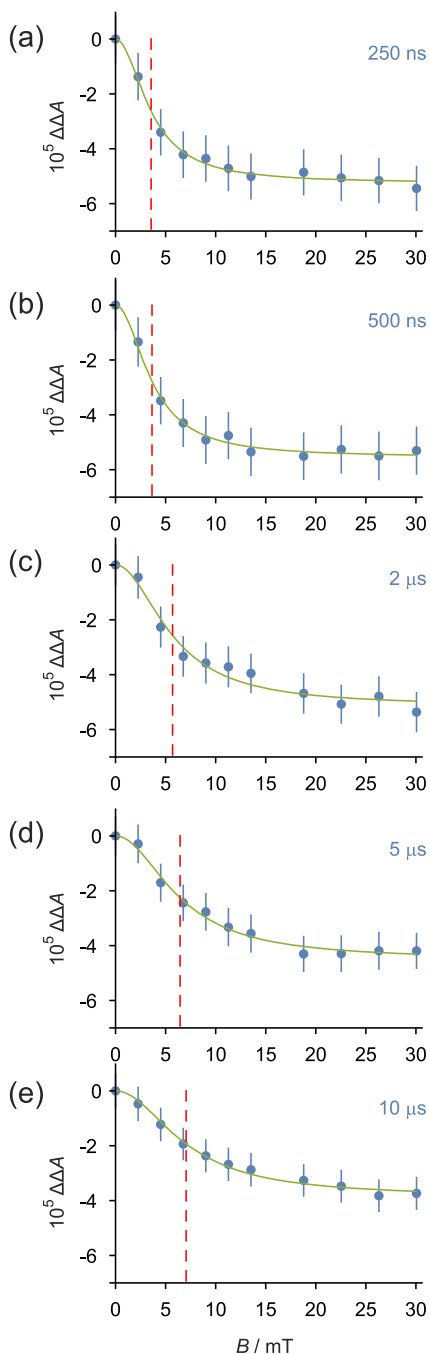
We have studied the radical pairs formed by photolysis of W369F mutants of *ErCry4a*, *GgCry4a*, and *CiCry4a* using a bespoke cavity ring-down spectroscopic technique described in Sec. II. The three *Cry4a* mutants contain a phenylalanine in place of the fourth tryptophan (W369) of the Trp-tetrad (Trp<sub>D</sub>, furthest from the FAD). The effect of the pump pulse is to excite the bound FAD chromophore, triggering three sequential electron transfers along the chain formed by the remaining three tryptophans (A, B, and C). The net result is the movement of an electron from the terminal tryptophan (Trp<sub>C</sub>) to the flavin, creating the  $[FAD^{\cdot-} Trp_C H^{\cdot+}]$  radical pair on a timescale too fast to be observed by the cavity ring-down spectrometer. Both of these radicals, as well as their protonated/deprotonated forms, FADH $\cdot$  and Trp<sub>C</sub> $\cdot$ , absorb at the wavelength of the probe light (530 nm).

Figure 1(a) shows the absorbance changes,  $\Delta A(t_d, 0)$ , measured in the absence of an applied magnetic field, for each of the proteins as a function of the pump-probe delay,  $t_d$ . The initial yield of radical pairs (highest for *ErCry4a* and lowest for *GgCry4a*) decays by  $\sim 50\%$  in the first 50  $\mu$ s, leaving a signal with lifetime greater than 100  $\mu$ s, attributed to the  $FAD^{\cdot-} Trp_C \cdot$  state [Fig. 1(c)] of the proteins. Also shown in Fig. 1(a) are fits to a biexponential model function,  $A_0 + A_1 \exp(-t_d/t_1) + A_2 \exp(-t_d/t_2)$ , for  $0 < t_d < 100 \mu$ s. In all



**FIG. 1.** Time-dependence of the absorbance changes at 530 nm for the W369F mutants of robin, chicken, and pigeon *Cry4a*. 150 measurements were made at each time-point. (a)  $\Delta A(t_d, 0)$  with fits to the biexponential model function,  $A_0 + A_1 \exp(-t_d/t_1) + A_2 \exp(-t_d/t_2)$ . The best-fit parameters are given in Table S2. The data could not satisfactorily be fitted to a mono-exponential model (see the supplementary material for details). (b)  $\Delta \Delta A(t_d, 30 \text{ mT})$ , the change in absorbance produced by a 30 mT magnetic field. The error bars in (b) represent the standard error of the mean; those in (a) are too small to see. (c) Simplified scheme showing the reactions of singlet and triplet states of  $[FAD^{\cdot-} Trp_C H^{\cdot+}]$  in W369F *Cry4a*. The curved arrows represent the coherent interconversion of the singlet and triplet radical pairs.

three proteins, the time constants are  $t_1 \approx 1 \mu s$  and  $t_2 = 10\text{--}15 \mu s$  (Table S2). We attribute the former to a combination of back electron transfer in the singlet radical pair,  $[FAD^{\cdot-} Trp_C H^{\cdot+}]$ , and deprotonation of  $Trp_C H^{\cdot+}$  to give  $FAD^{\cdot-} Trp_C \cdot$  [Fig. 1(c)]. Competition between these two reactions, mediated by coherent singlet-triplet interconversion, gives rise to the magnetic field effects shown in Fig. 1(b). The magnetic field ( $B = 30 \text{ mT}$ ) reduces the



**FIG. 2.** Magnetic field-dependence of the light-induced changes in the absorbance of *ErCry4a* W369F at pump-probe delays of (a) 250 ns, (b) 500 ns, (c) 2  $\mu$ s, (d) 5  $\mu$ s, (e) 10  $\mu$ s. The green lines are fits to Eq. (2). In each panel, the error bars represent the standard error of the mean. The dashed red lines mark the values of  $B_{1/2}(t_d)$  obtained by fitting to Eq. (2). Measurements with 100  $\mu$ s and 1 ms delays (not shown) had substantially lower signal-to-noise ratio and did not give reliable values of  $B_{1/2}(t_d)$ .

**TABLE I.** Values of  $B_{1/2}(t_d)$  (in mT) for Cry4a W369F mutants.<sup>a</sup>

$t_d$ ( $\mu$ s)	Robin	Chicken	Pigeon
0.25	$3.55 \pm 0.16$	$3.39 \pm 0.26$	$5.10 \pm 0.58$
0.50	$3.64 \pm 0.17$	$4.50 \pm 0.32$	$4.35 \pm 0.26$
2.0	$5.70 \pm 0.48$	$4.91 \pm 0.44$	$6.75 \pm 0.56$
5.0	$6.45 \pm 0.35$	$5.97 \pm 0.61$	$7.08 \pm 0.53$
10.0	$7.05 \pm 0.32$	$5.40 \pm 0.42$	$9.33 \pm 0.97$

<sup>a</sup>Obtained from the data in Figs. 2 and S1. The error estimates were calculated using the method of Cramér–Rao lower bounds (supplementary material<sup>38,39</sup>). A plot of these data can be found in Sec. III C.

concentration of radicals by inhibiting singlet–triplet interconversion, thereby boosting recombination of singlet pairs to the ground state.<sup>22</sup> The absolute magnetic field effects are in the order robin > pigeon > chicken and the peak relative magnetic field effects, defined as the maximum values of  $|\Delta\Delta A(t_d, 30 \text{ mT})/\Delta A(t_d, 0)|$ , are 21% for robin, 17% for pigeon, and 14% for chicken. The smaller variation in the relative effects among the three proteins reflects the differences in their radical yields [Fig. 1(a)].

In a separate series of experiments, we measured the change in absorbance produced by magnetic fields in the range  $0 < B < 30$  mT at five pump–probe delays ( $0 < t_d < 10 \mu$ s) spanning the decay of the fast component ( $t_1 \approx 1 \mu$ s) of the kinetics in Fig. 1(a). The results for the robin protein are shown in Fig. 2. Similar data were measured for chicken and pigeon Cry4a W369F (Fig. S1). All three proteins display the sigmoidal magnetic field-dependence characteristic of the radical pair mechanism.<sup>34</sup> Also shown in Fig. 2 are fits of the data to a Lorentzian model,

$$f(t_d) = h(t_d) \left[ 1 - \frac{1}{1 + (B/B_{1/2}(t_d))^2} \right], \quad (2)$$

in which  $h(t_d)$  is the limiting value of  $\Delta\Delta A(t_d, B)$  at high field (in practice,  $\sim 30$  mT). The values of  $B_{1/2}(t_d)$  so obtained are given in Table I. The trend for all three proteins is for  $B_{1/2}(t_d)$  to increase with increasing pump–probe delay.

The values of  $B_{1/2}(t_d)$  in Table I may be compared with an approximate expression, proposed by Weller,<sup>32</sup> in which  $B_{1/2}$  is assumed to be determined solely by isotropic hyperfine interactions as follows:

$$B_{1/2} = 2\sqrt{3} \left( \frac{\sigma_{\text{FAD}}^2 + \sigma_{\text{TRP}}^2}{\sigma_{\text{FAD}} + \sigma_{\text{TRP}}} \right). \quad (3)$$

In Eq. (3),  $\sigma_{\text{FAD}}$  and  $\sigma_{\text{TRP}}$  are the effective isotropic hyperfine interactions in the two radicals, defined as

$$\sigma_j = \sqrt{\frac{1}{3} \sum_i a_{ji}^2 I_j(I_j + 1)}. \quad (4)$$

Here,  $a_{ji}$  and  $I_j$  are, respectively, the isotropic hyperfine interaction and the spin quantum number ( $1/2$  for  $^1\text{H}$ , 1 for  $^{14}\text{N}$ ) of nuclear spin  $i$  in radical  $J$ . Using hyperfine data for  $\text{FAD}^{\cdot-}$  and

TrpH<sup>+</sup> calculated using Gaussian03,<sup>33,40</sup> we obtain  $\sigma_{\text{FAD}} = 0.70$  mT and  $\sigma_{\text{Trp}} = 0.97$  mT, and, hence [Eq. (3)],  $B_{1/2} = 3.0$  mT. A recent and much more sophisticated treatment of the spin dynamics of [FAD<sup>-</sup> TrpH<sup>+</sup>] radical pairs gave  $B_{1/2} = 2.46$  mT.<sup>34</sup> All the values of  $B_{1/2}(t_d)$  in Table I exceed 3.0 mT, suggesting that electron spin relaxation influences the spin dynamics of the radical pair<sup>33</sup> and hence its magnetic sensitivity.

## B. Spin dynamics simulations of magnetic field effects

In an attempt to understand the time-dependence of the magnetic field effects, we have performed spin dynamics simulations using the semiclassical approach proposed by Schulten and Wolynes.<sup>41</sup> Briefly, we consider a radical pair created in a singlet state and able to react from its singlet and triplet states with equal rate constants,  $k$ , to give distinct products (the “exponential model,”<sup>42</sup> see also the supplementary material). The effects of hyperfine interactions on the coherent spin dynamics were included by

averaging over isotropic Gaussian distributions of hyperfine fields (mean zero and standard deviation  $\sigma_{\text{FAD}}$  or  $\sigma_{\text{Trp}}$ , using  $10^4$  Monte Carlo samples). Exchange and dipolar interactions between the radicals were ignored. The magnetic field effect was assessed by means of the quantum yield of the product formed from the triplet state of the radical pair,

$$\Phi_{\text{T}}(t_d, B) = k \int_0^{t_d} p_{\text{T}}(t, B) e^{-kt} dt. \quad (5)$$

In Eq. (5),  $p_{\text{T}}(t, B)$  is the probability that the radical pair is in its triplet state at time  $t$  when subject to a magnetic field  $B$  in the absence of the product-forming reactions. We refer to  $\Phi_{\text{T}}(t_d, B)$  as the “triplet yield” and use it here so that the magnetic field effects have the same sign as in Fig. 2, i.e.,  $\Phi_{\text{T}}(t_d, 0) > \Phi_{\text{T}}(t_d, B)$ .

Anticipating that electron spin relaxation could be the source of the time-dependence of  $B_{1/2}(t_d)$ , the simulations included either singlet–triplet dephasing (STD<sup>35,43,44</sup>) or, for comparison, random

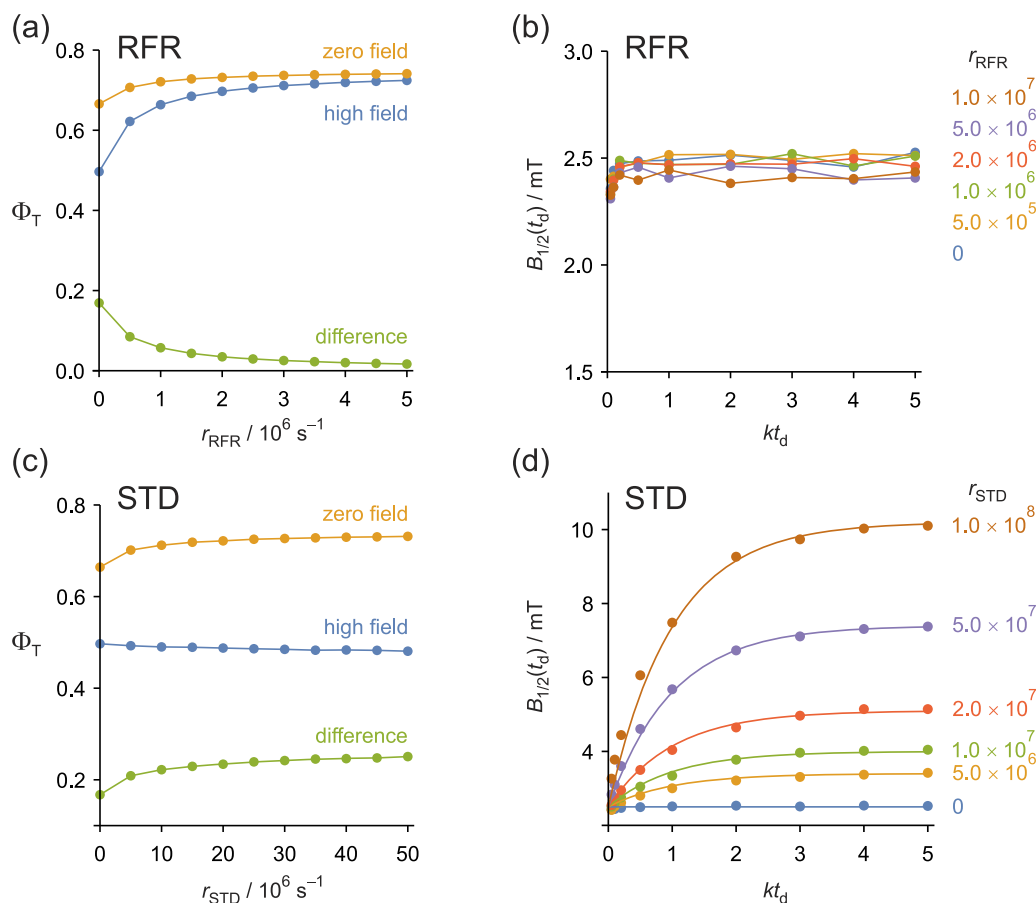


**FIG. 3.** Calculated effects of the spin relaxation mechanisms, RFR [(a) and (b)] and STD [(c) and (d)], on  $\Phi_{\text{T}}(t_d, B)$  at  $t_d \rightarrow \infty$  [(a) and (c)], and on  $B_{1/2}(t_d)$  [(b) and (d)], with  $k = 10^6 \text{ s}^{-1}$ . The numbers on the right-hand side of (b) and (d) are values of the relevant relaxation rate constant in  $\text{s}^{-1}$ . “High field” in (a) and (c) denotes the limiting behavior in a magnetic field much stronger than the effective hyperfine interactions. The smooth lines in (d) are fits of the simulated  $B_{1/2}(t_d)$  values to Eqs. (6) and (7). The noise on the  $B_{1/2}$  values plotted in (b) and (d) arises from the Monte Carlo sampling.



fields relaxation (RFR<sup>25</sup>). STD can arise from fluctuations in the electron exchange interaction brought about by stochastic modulation of the inter-radical separation or by reversible electron hopping between sites with different radical-radical separations. STD has been invoked previously as an explanation for the unexpectedly large  $B_{1/2}$  values observed for Cry1 from the plant *Arabidopsis thaliana* and for DNA photolyase from *E. coli*.<sup>33</sup> RFR is a generic mechanism in which the two electron spins are relaxed isotropically with equal rate constants. Although its quantitative applicability is certainly questionable, RFR has been used in the past to model the effects of stochastic modulation of hyperfine interactions caused by fluctuations in dihedral angles and librational motions of the radicals within the protein.<sup>35</sup> The superoperators used to model the effects of RFR and STD are given in the supplementary material.

The results of these simulations are presented in two forms. Figures 3(a) and 3(c) show the final triplet yield ( $t_d \rightarrow \infty$ ) at zero field,  $\Phi_T(\infty, 0)$ , at high field,  $\Phi_T(\infty, \infty)$ , and their difference, plotted as a function of the relaxation rate constant ( $r_{\text{RFR}}$  or  $r_{\text{STD}}$ ). Figures 3(b) and 3(d) show  $B_{1/2}(t_d)$ , plotted as a function of the pump-probe delay scaled by the recombination rate constant for a selection of values of  $r_{\text{RFR}}$  or  $r_{\text{STD}}$ . In all four panels of Fig. 3, the value of  $k$  ( $10^6 \text{ s}^{-1}$ ) was chosen to match the reciprocal of the  $\sim 1 \mu\text{s}$  time constant measured for the three proteins (Fig. 1 and Table S2).

The RFR mechanism attenuates the magnetic field effect,  $\Phi_T(0) - \Phi_T(\infty)$  [Fig. 3(a)], and produces no significant change in  $B_{1/2}$  or dependence on  $t_d$  [Fig. 3(b)]. By relaxing all three Cartesian spin components of the two electrons, this mechanism equilibrates all electron spin degrees of freedom and strongly attenuates the magnetic field effect as soon as the spin relaxation rate constant,  $r_{\text{RFR}}$ , approaches and exceeds the recombination rate constant,  $k$ . An alternative model of low-field spin relaxation of cryptochrome-based radical pairs is discussed in the supplementary material.

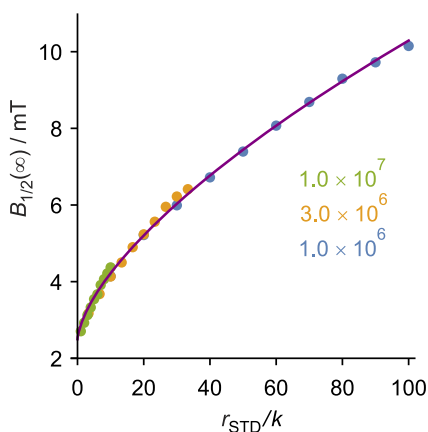


**FIG. 4.** Dependence of calculated  $B_{1/2}(\infty)$  on  $r_{\text{STD}}/k$  for three values of  $k$  (in  $\text{s}^{-1}$ ), as indicated. The purple line is Eq. (7).

By contrast, the STD mechanism preserves the magnetic field effect [Fig. 3(c)], and even increases it slightly, and gives a pronounced dependence of  $B_{1/2}(t_d)$  on both  $kt_d$  and  $r_{\text{STD}}$  [Fig. 3(d)]. Compared to RFR, the STD effects are much less sensitive to the relaxation rate:  $r_{\text{RFR}} = 5 \times 10^6 \text{ s}^{-1}$  almost destroys the magnetic field-dependence [Fig. 3(a)] while the same value of  $r_{\text{STD}}$  has very little effect [Fig. 3(c)]. These effects stem from the selective relaxation of a portion of the electron spin space (singlet-triplet coherences) as discussed in more detail below.

The growth of  $B_{1/2}(t_d)$  as a function of  $t_d$  [Fig. 3(d)] was found to follow the empirical equations given by

$$B_{1/2}(t_d) \approx [2.5 - B_{1/2}(\infty)] \exp(-kt_d) + B_{1/2}(\infty), \quad (6)$$

$$B_{1/2}(\infty) \approx 2.5 + 0.37 \left( \frac{r_{\text{STD}}}{k} \right)^{0.66}, \quad (7)$$

in which the values of  $B_{1/2}(t_d)$  and  $B_{1/2}(\infty)$  are in millitesla. The dependence of  $B_{1/2}(\infty)$  on  $r_{\text{STD}}/k$  [Eq. (7)], for three values of  $k$ , can be seen in Fig. 4. The value of  $B_{1/2}$  in the absence of STD ( $\sim 2.5 \text{ mT}$ ) is  $\sim 0.5 \text{ mT}$  smaller than predicted by Weller's formula, Eq. (3).<sup>34</sup>

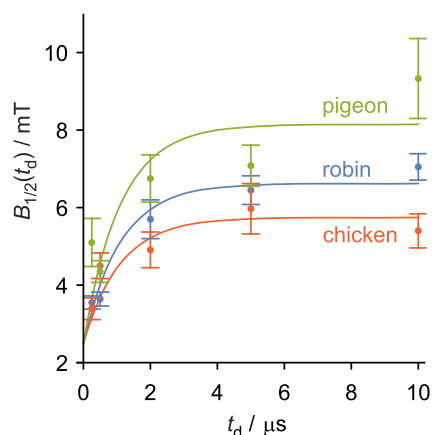


**FIG. 5.**  $B_{1/2}(t_d)$  data (Table I) as a function of  $t_d$  together with fits to Eqs. (6) and (7) with  $k^{-1} = 1.0 \mu\text{s}$ . See Table II for fit parameters. A discussion of the reliability of these fits can be found in the supplementary material.

**TABLE II.** Values of  $r_{\text{STD}}$  and  $B_{1/2}(\infty)$ .<sup>a</sup>

	Robin	Chicken	Pigeon
$r_{\text{STD}}/10^7 \text{ s}^{-1b}$	$3.8 \pm 0.2$	$2.6 \pm 0.3$	$6.1 \pm 0.6$
$B_{1/2}(\infty)/\text{mT}^c$	$6.6 \pm 0.2$	$5.7 \pm 0.2$	$8.1 \pm 0.3$

<sup>a</sup>Obtained from fitting the data in Table I (displayed in Fig. 5) to Eqs. (6) and (7), using  $k^{-1} = 1.0 \mu\text{s}$ .

<sup>b</sup>The error estimates were obtained using the method of Cramér-Rao lower bounds (supplementary material<sup>38,39</sup>).

<sup>c</sup>The values of  $B_{1/2}(\infty)$  were obtained from the corresponding values of  $r_{\text{STD}}$  using Eq. (7).

### C. Analysis of time-dependent magnetic field effects

Noting that the RFR mechanism has no effect on  $B_{1/2}$  within the Schulten–Wolynes model [Fig. 3(b)], we henceforth ignore it and focus on STD as the likely source of the  $t_d$ -dependence. The experimental values of  $B_{1/2}(t_d)$  (Table I) were therefore fitted to Eqs. (6) and (7) by varying  $r_{\text{STD}}$ , with  $k^{-1} = t_1 = 1.0 \mu\text{s}$ . Values of  $B_{1/2}(\infty)$  were then obtained using Eq. (7). The results are shown in Fig. 5 and Table II. (A more sophisticated analysis, outlined in the supplementary material, gives similar values for  $r_{\text{STD}}$ .) The values of  $r_{\text{STD}}$  for the three proteins are in the range  $3\text{--}6 \times 10^7 \text{ s}^{-1}$ .

### D. Origin of time-dependent magnetic field effects

In Sec. III A, we saw that magnetic field effects as large as 15%–20% can persist in the presence of singlet–triplet dephasing that is 30–60 times faster than radical recombination. In this section, we review the origins of this effect and of the time-dependence of  $B_{1/2}(t_d)$  by means of a “toy” model due to Maeda and Miura<sup>44,45</sup> in which the four electron spin states (S,  $T_{+1}$ ,  $T_0$ ,  $T_{-1}$ ) are reduced to a two-level system, {S, T}, where T represents either  $T_{+1}$  or  $T_{-1}$ . We consider first the random fields mechanism and then move on to the more interesting effects of singlet–triplet dephasing. Details are given in the supplementary material.

Following Maeda and Miura,<sup>44,45</sup> we consider a spin Hamiltonian,

$$\hat{H} = \omega |T\rangle\langle T| + \frac{1}{2}q |S\rangle\langle T| + \frac{1}{2}q |T\rangle\langle S|, \quad (8)$$

in which  $\omega$  and  $q$  parametrize, respectively, the interaction of the electron spins with an external magnetic field and with the magnetic field resulting from the hyperfine interactions with nuclear spins. The former removes the degeneracy of the S and T states; the latter results in coherent S  $\leftrightarrow$  T interconversion. Ignoring chemical reactions and spin relaxation, the time-dependent triplet fraction, for a

radical pair formed in the S state, is given exactly by (supplementary material)

$$p_{\text{T}}(t) = \frac{1}{2} - \frac{1}{2} \left[ \frac{\omega^2 + q^2 \cos(\sqrt{\omega^2 + q^2} t)}{\omega^2 + q^2} \right]. \quad (9)$$

When the Zeeman interaction greatly exceeds the hyperfine interactions ( $\omega \gg q$ ), S  $\leftrightarrow$  T mixing is inefficient and the triplet probability remains close to zero and has an oscillatory component of low amplitude,  $q^2/(\omega^2 + q^2)$ , and frequency,  $(\omega^2 + q^2)^{1/2} \approx \omega$ .

The effect of the RFR mechanism is to relax the diagonal elements of the density operator,  $\hat{\rho}$ , toward  $\frac{1}{2}$  and the off-diagonal elements toward zero,

$$\begin{aligned} \frac{d(\rho_{\text{SS}} - \rho_{\text{TT}})}{dt} &= -2r_{\text{RFR}}(\rho_{\text{SS}} - \rho_{\text{TT}}); \\ \frac{d\rho_{\text{ST}}}{dt} &= -r_{\text{RFR}}\rho_{\text{ST}}; \quad \frac{d\rho_{\text{TS}}}{dt} = -r_{\text{RFR}}\rho_{\text{TS}}, \end{aligned} \quad (10)$$

where  $\rho_{jk} = \langle j|\hat{\rho}|k\rangle$ . Treating the hyperfine field,  $q$ , as a perturbation, i.e.,  $\Omega^2 = q^2/(r^2 + \omega^2) \ll 1$ , the triplet fraction, to second order in  $q$  (supplementary material), is given by

$$p_{\text{T}}(t) \approx \frac{1}{2} - \frac{1}{2} \left[ \frac{\exp(-2r_{\text{RFR}}t) + \Omega^2 \cos(\omega t) \exp(-r_{\text{RFR}}t)}{1 + \Omega^2} \right]. \quad (11)$$

For the STD mechanism, only the singlet–triplet coherences are relaxed,

$$\frac{d\rho_{\text{ST}}}{dt} = -r_{\text{STD}}\rho_{\text{ST}}; \quad \frac{d\rho_{\text{TS}}}{dt} = -r_{\text{STD}}\rho_{\text{TS}}, \quad (12)$$

and the triplet probability (supplementary material) becomes

$$p_{\text{T}}(t) \approx \frac{1}{2} - \frac{1}{2} \left[ \frac{\exp(-r_{\text{STD}}\Omega^2 t) + \Omega^2 \cos(\omega t) \exp(-r_{\text{STD}}t)}{1 + \Omega^2} \right]. \quad (13)$$

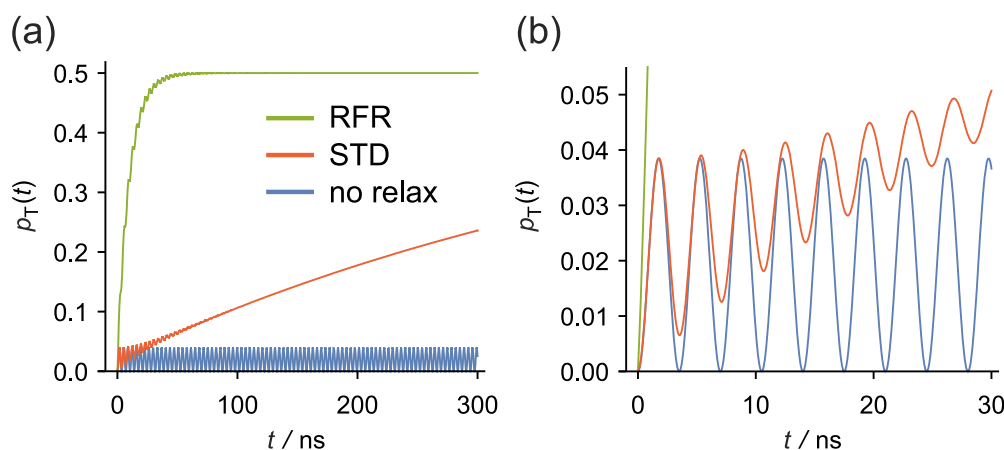


**FIG. 6.** (a) Time-dependence of the triplet fraction calculated using the toy model described in the text. Blue, green, and red traces correspond to Eqs. (9), (11), and (13), respectively. Calculated with  $q = 2 \text{ mT}$ ,  $\omega = 10 \text{ mT}$ ,  $r_{\text{STD}} = r_{\text{RFR}} = 5 \times 10^7 \text{ s}^{-1}$ . Radical reactions are not included. (b) Expanded version of (a) showing the time-dependence in the first 30 ns.



Comparing Eqs. (11) and (13), it is clear that both relaxation mechanisms result in damped low-amplitude oscillations (frequency  $\omega$ , amplitude  $\sim \Omega^2 \ll 1$ , and damping rate constant  $r_{\text{RFR}}$  or  $r_{\text{STD}}$ ) together with an exponential rise of the triplet probability toward 0.5. The latter may be seen more clearly by simplifying Eqs. (11) and (13), using  $\Omega^2 \ll 1$ , to obtain

$$p_{\text{T}}(t) \approx \frac{1}{2} [1 - \exp(-2r_{\text{RFR}}t)] \quad (14)$$

for RFR and

$$p_{\text{T}}(t) \approx \frac{1}{2} [1 - \exp(-r_{\text{STD}}\Omega^2 t)] \quad (15)$$

for STD.<sup>44</sup> As  $\Omega^2 \ll 1$ , the approach of the triplet fraction to equilibrium should be much faster for RFR than for STD for similar values of  $r_{\text{RFR}}$  and  $r_{\text{STD}}$ .

The difference between the two relaxation mechanisms may be seen in Fig. 6, which shows  $p_{\text{T}}(t)$  calculated with RFR, STD, and no relaxation. The values chosen for  $q$ ,  $\omega$ , and  $r_{\text{RFR}} = r_{\text{STD}}$  correspond to  $\Omega^2 = 0.04$ . When there is no spin relaxation, the triplet probability remains close to zero because the strong Zeeman interaction ( $\omega \gg q$ ) inhibits coherent singlet–triplet interconversion. The RFR mechanism relaxes  $p_{\text{T}}(t)$  rapidly toward 0.5 with rate constant  $2r_{\text{RFR}} = 10^8 \text{ s}^{-1}$  [Eq. (14)]. STD by contrast damps the S  $\leftrightarrow$  T oscillations rapidly but causes  $p_{\text{T}}(t)$  to grow much more slowly. For the parameters chosen for Fig. 6, this process occurs with a rate constant  $r_{\text{STD}}\Omega^2 = 2 \times 10^6 \text{ s}^{-1}$ , 50 times slower than  $2r_{\text{RFR}}$ . The result of STD under these conditions is an exponential approach to equilibrium with a rate constant ( $r_{\text{STD}}\Omega^2$ ) that depends on the applied magnetic field and the hyperfine interactions via  $\Omega^2 = q^2/(r_{\text{STD}}^2 + \omega^2)$ .

Finally, Eq. (15) sheds light on the magnetic field effects in the presence of STD. Using the exponential model again (spin-selective S and T pairs recombine with rate constant,  $k$ ), the ultimate triplet yield is

$$\Phi_{\text{T}}(\omega) = k \int_0^{\infty} p_{\text{T}}(t') \exp(-kt') dt' = \frac{r_{\text{STD}}\Omega^2}{2(k + r_{\text{STD}}\Omega^2)}. \quad (16)$$

Equation (16) predicts the expected sigmoidal dependence on the magnetic field intensity,  $\omega$ , with a  $B_{1/2}$ -like parameter, defined by  $\Phi_{\text{S}}(\omega_{1/2}) = \frac{1}{2} [\Phi_{\text{S}}(0) + \Phi_{\text{S}}(\infty)]$ , of  $\omega_{1/2} \approx q(r_{\text{STD}}/k)^{0.5}$  when  $q^2 \gg k r_{\text{STD}}$ . Remembering that this expression comes from a highly approximate model of the spin dynamics, it is notable that the dependence of  $\omega_{1/2}$  on  $(r_{\text{STD}}/k)^{0.5}$  is so similar to the empirical dependence of  $B_{1/2}(\infty)$  on  $(r_{\text{STD}}/k)^{0.66}$  in Eq. (7).

## IV. DISCUSSION

### A. Comparison of RFR and STD relaxation mechanisms

The pronounced difference between the effects of the RFR and STD relaxation mechanisms stems from the selective nature of the latter. RFR indiscriminately drives both the populations of the singlet and triplet states ( $\rho_{\text{SS}}$  and  $\rho_{\text{TT}}$ ) and the singlet–triplet coherences ( $\rho_{\text{ST}}$  and  $\rho_{\text{TS}}$ ) toward equilibrium, all at the same rate [Eq. (10)]. STD, by contrast, directly relaxes the coherences [Eq. (12)] but only

has an indirect effect on the populations. In the absence of spin relaxation, the hyperfine interactions convert  $\rho_{\text{SS}}$  into  $\rho_{\text{TT}}$  via  $\rho_{\text{ST}}$  and  $\rho_{\text{TS}}$ , a process that may be represented by

$$\rho_{\text{SS}} \rightarrow i(\rho_{\text{ST}} - \rho_{\text{TS}}) \rightarrow \rho_{\text{TT}}, \quad (17)$$

where  $i(\rho_{\text{ST}} - \rho_{\text{TS}})$  is the imaginary part of the coherence (supplementary material). If STD is efficient, the intermediate coherence dephases rapidly before much of it can be converted into  $\rho_{\text{TT}}$ . The result is that STD reduces the rate at which singlet is converted to triplet (as shown in Fig. 6). Although the dephasing itself may be fast ( $\sim 5 \times 10^7 \text{ s}^{-1}$ , Table II), its effect on the populations can be much slower ( $\sim 1 \times 10^6 \text{ s}^{-1}$  here). This outcome is reminiscent of a model in which the spin–lattice relaxation time ( $T_1$ ) greatly exceeds the spin–spin relaxation time ( $T_2$ ): see the supplementary material.

### B. Origin of singlet–triplet dephasing in Cry4a

The time-dependent magnetic field effects reported above appear to be consistent with singlet–triplet dephasing.<sup>25,43,44</sup> There seems to be no other physically plausible relaxation mechanism that would cause  $B_{1/2}$  to increase with the pump–probe delay. However, what is its origin?

Singlet–triplet coherences decay as a result of stochastic variations in the singlet–triplet energy gap, which in turn arise from fluctuations in the exchange interaction of the two unpaired electrons.<sup>25</sup> One way in which this could occur is from variations in the separation of the radicals,  $R$ , within the protein as a result of thermal motion. Even though it is a steep function of the radical–radical distance, and therefore sensitive to small changes in  $R$ , the exchange interaction is so small for the flavin–tryptophan radical pairs in Cry4a ( $< 10 \mu\text{T}$ <sup>22</sup>) that it is very unlikely to be an important source of dephasing.

A more credible mechanism is electron hopping. This possibility was previously suggested to account for the larger-than-expected  $B_{1/2}$  values measured for *A. thaliana* Cry1 and *E. coli* photolyase.<sup>33</sup> Specifically, an electron was considered to jump rapidly from Trp<sub>B</sub>, the second component of the Trp-triad, onto Trp<sub>C</sub>H<sup>+</sup> and back again,



This would result in a strong modulation of the exchange interaction experienced by the FAD<sup>·-</sup> radical, which is  $\sim 4.6 \text{ \AA}$  closer to Trp<sub>B</sub>H<sup>+</sup> than to Trp<sub>C</sub>H<sup>+</sup>.<sup>19,22</sup> We refer to the states on the left- and right-hand sides of Eq. (18) as RP<sub>C</sub> and RP<sub>B</sub>, respectively. The exchange interaction in RP<sub>B</sub> has been estimated to be as large as  $\sim 1.0 \text{ T}$ .<sup>46</sup>

The effect of this reversible electron hopping process on the spin dynamics may be seen as follows:<sup>43</sup> Let  $k_{\text{BC}}$  and  $k_{\text{CB}}$  be the rate constants for RP<sub>B</sub>  $\rightarrow$  RP<sub>C</sub> and RP<sub>C</sub>  $\rightarrow$  RP<sub>B</sub>, respectively, and suppose that  $k_{\text{BC}} \gg k_{\text{CB}}$  such that RP<sub>B</sub> is short-lived and has a much lower equilibrium concentration than RP<sub>C</sub>. This limit is consistent with EPR measurements of the distance between the flavin and tryptophan radicals in robin Cry4a, which show that any equilibrium between RP<sub>B</sub> and RP<sub>C</sub> strongly favors RP<sub>C</sub>.<sup>22</sup> Under these conditions, and assuming that the spin interactions in RP<sub>B</sub> are dominated

by its large exchange interaction ( $J_B$ ), the net effect of the electron hopping (according to Shushin<sup>43</sup>) is to introduce singlet–triplet dephasing with rate constant (supplementary material)

$$r_{\text{STD}} = \frac{4J_B^2 k_{\text{CB}}}{4J_B^2 + k_{\text{BC}}^2} \quad (19)$$

and an additional exchange interaction in  $\text{RP}_C$  with strength

$$J_{\text{STD}} = \frac{J_B k_{\text{BC}} k_{\text{CB}}}{4J_B^2 + k_{\text{BC}}^2}. \quad (20)$$

Similar expressions have been obtained by Haberkorn.<sup>47,48</sup> Reliable experimental measurements of  $k_{\text{BC}}$ ,  $k_{\text{CB}}$ , and  $J_B$  are not available. If  $J_B \gg k_{\text{BC}}$ , then Eq. (19) gives  $r_{\text{STD}} \approx k_{\text{CB}}$ , suggesting that the rate constant for  $\text{RP}_C \rightarrow \text{RP}_B$  is in the range  $3\text{--}6 \times 10^7 \text{ s}^{-1}$  (Table II). In the same limit, Eq. (20) gives  $J_{\text{STD}} \ll k_{\text{CB}}$ , implying a negligible effect on the spin dynamics.

The assumption that  $k_{\text{BC}} \gg k_{\text{CB}}$  and the resulting value of  $k_{\text{CB}}$  ( $3\text{--}6 \times 10^7 \text{ s}^{-1}$ ) are only partially supported by estimates based on molecular dynamics simulations of *ErCry4a*. In the work of Xu *et al.*,  $k_{\text{BC}}/k_{\text{CB}} \approx 6 \times 10^4$  and  $k_{\text{CB}} \approx 9 \times 10^5 \text{ s}^{-1}$  were obtained.<sup>22</sup> Given the approximate nature of these calculations, it cannot be excluded that  $k_{\text{CB}}$  could be as large as  $3\text{--}6 \times 10^7 \text{ s}^{-1}$ .

### C. Relevance to wild type proteins

The experiments reported here were performed exclusively on mutants of *Cry4a* in which electron transfer beyond  $\text{Trp}_C\text{H}$  was blocked by replacement of  $\text{Trp}_D\text{H}$  by phenylalanine such that  $[\text{FAD}^{\cdot-} \text{Trp}_C\text{H}^{\cdot+}]$  ( $\text{RP}_C$ ) produces the magnetic field effects. In the wild type (WT) proteins, by contrast, all four components of the Trp-tetrad are active in electron transfer and the dominant charge-separated state is  $[\text{FAD}^{\cdot-} \text{Trp}_D\text{H}^{\cdot+}]$  ( $\text{RP}_D$ ). As shown previously for *ErCry4a*,<sup>22</sup>  $\text{RP}_D$  shows smaller magnetic field effects *in vitro* than  $\text{RP}_C$ , an effect attributed to its larger radical–radical separation and hence slower recombination.<sup>22</sup> This made it difficult for us to obtain reliable values of  $B_{1/2}$  for the WT proteins and impossible to determine whether there is any dependence of  $B_{1/2}$  on the pump–probe delay.

At first sight, one would not expect  $\text{RP}_B \rightleftharpoons \text{RP}_C$  electron hopping to have much of an effect in the WT proteins because of the low population of the  $\text{RP}_C$  state. If interconversion of  $\text{RP}_B$  and  $\text{RP}_C$  is indeed the origin of STD in the mutants, it would therefore not appear to be important for the WT proteins. However, the possibility (discussed in Ref. 35) that  $\text{RP}_C \rightleftharpoons \text{RP}_D$  electron hopping is significant *in vivo* could conceivably allow all three radical pairs to interconvert, i.e.,  $\text{RP}_B \rightleftharpoons \text{RP}_C \rightleftharpoons \text{RP}_D$ , and hence give rise to STD effects. This possibility must remain speculative pending further measurements on the WT proteins.

Finally, the differences in magnetic field effects seen for robin, chicken, and pigeon *Cry4a*'s<sup>22</sup> presumably arise from the amino acid sequence differences among the three proteins in the neighborhood of the FAD and the Trp-tetrad and could therefore be linked to differences in spin relaxation rates. However, the rather similar STD rate constants found here for the three W369F mutants suggest that one may need to look elsewhere for an explanation of this difference in magnetic sensitivity. What can be said is that strong

magnetic field effects in cryptochromes are not incompatible with fast singlet–triplet dephasing.

### SUPPLEMENTARY MATERIAL

The supplementary material includes data for chicken and pigeon *Cry4a* corresponding to Fig. 2, the parameter values obtained from fitting the data in Fig. 1(a), and information on the primers used for site-specific mutagenesis; analysis of the data in Figs. 1(a) and 5; the Cramér–Rao lower bounds method; our analysis of time-dependent magnetic field effects; spin relaxation mechanisms and superoperators; the Maeda–Miura model; and the origin of Eqs. (19) and (20).

### ACKNOWLEDGMENTS

We are grateful for the financial support provided by the European Research Council (under the European Union's Horizon 2020 research and innovation program, Grant Agreement No. 810002, Synergy Grant: *QuantumBirds*), the Deutsche Forschungsgemeinschaft, DFG (Grant Nos. SFB 1372, *Magnetoreception and navigation in vertebrates* and GRK 1885, *Molecular basis of sensory biology*), and the Office of Naval Research Global (Award No. N62909-19-1-2045). M.J.G. thanks the Biotechnology and Biological Sciences Research Council, Grant No. BB/M011224/1 and Oxford University's Clarendon Fund. J.L. is grateful to Tom Fay for helpful advice. We are also grateful to an anonymous reviewer for comments on an earlier version of the manuscript.

### AUTHOR DECLARATIONS

#### Conflict of Interest

The authors have no conflicts to disclose.

#### Author Contributions

**Matthew J. Golesworthy:** Investigation (lead). **Tilo Zollitsch:** Investigation (lead). **Jiate Luo:** Investigation (lead). **Dan Selby:** Investigation (supporting). **Lauren E. Jarocho:** Investigation (supporting). **Kevin B. Henbest:** Investigation (supporting). **Olivier Paré-Labrosse:** Investigation (supporting). **Rabea Bartölke:** Investigation (supporting). **Jessica Schmidt:** Investigation (supporting). **Jingjing Xu:** Investigation (supporting). **Henrik Mouritsen:** Conceptualization (equal); Supervision (equal). **P. J. Hore:** Conceptualization (equal); Supervision (equal); Writing – original draft (lead). **Christiane R. Timmel:** Conceptualization (equal); Supervision (equal). **Stuart R. Mackenzie:** Conceptualization (equal); Supervision (equal).

### DATA AVAILABILITY

The data that support the findings of this study are available from the corresponding authors upon reasonable request.

### REFERENCES

<sup>1</sup>W. Wiltschko and F. W. Merkel, "Orientierung zugunruhiger rotkehlchen im statischen magnetfeld," *Verh. der Deutsch. Zool. Ges.* **59**, 362 (1966).

- <sup>2</sup>W. Wiltschko and R. Wiltschko, "Magnetic compass of European robins," *Science* **176**, 62 (1972).
- <sup>3</sup>R. Wiltschko and W. Wiltschko, *Magnetic Orientation in Animals* (Springer Verlag, Berlin, 1995).
- <sup>4</sup>G. C. Nordmann, T. Hochstoeger, and D. A. Keays, "Magnetoreception—A sense without a receptor," *PLoS Biol.* **15**, e2003234 (2017).
- <sup>5</sup>H. Mouritsen, "Long-distance navigation and magnetoreception in migratory animals," *Nature* **558**, 50 (2018).
- <sup>6</sup>S. Johnsen, K. J. Lohmann, and E. J. Warrant, "Animal navigation: A noisy magnetic sense?," *J. Exp. Biol.* **223**, jeb164921 (2020).
- <sup>7</sup>R. Wiltschko, C. Nießner, and W. Wiltschko, "The magnetic compass of birds: The role of cryptochrome," *Front. Physiol.* **12**, 667000 (2021).
- <sup>8</sup>N. Karki, S. Vergish, and B. D. Zoltowski, "Cryptochromes: Photochemical and structural insight into magnetoreception," *Protein Sci.* **30**, 1521 (2021).
- <sup>9</sup>G. Durieux and M. Liedvogel, in *Position, Navigation, and Timing Technologies in the 21st Century: Integrated Satellite Navigation, Sensor Systems, and Civil Applications*, edited by Y. T. J. Morton, F. van Diggelen, and J. J. Spilker (John Wiley and Sons, Inc., 2021), p. 1689.
- <sup>10</sup>A. Bradlaugh, A. L. Munro, A. R. Jones, and R. A. Baines, "Exploiting the fruitfly, *Drosophila melanogaster*, to identify the molecular basis of cryptochrome-dependent magnetosensitivity," *Quantum Rep.* **3**, 127 (2021).
- <sup>11</sup>R. Kavet and J. Brain, "Cryptochromes in mammals and birds: Clock or magnetic compass?," *Physiology* **36**, 183 (2021).
- <sup>12</sup>S. Y. Wong, A. Frederiksen, M. Hanic, F. Schuhmann, G. Grüning, P. J. Hore, and I. A. Solov'yov, "Navigation of migratory songbirds: A quantum magnetic compass sensor," *Neuroforum* **27**, 141 (2021).
- <sup>13</sup>N. F. Putman, "Magnetosensation," *J. Comp. Physiol., A* **208**, 1 (2022).
- <sup>14</sup>A. A. Bradlaugh, G. Fedele, A. L. Munro, C. N. Hansen, J. M. Hares, S. Patel, C. P. Kyriacou, A. R. Jones, E. Rosato, and R. A. Baines, "Essential elements of radical pair magnetosensitivity in *Drosophila*," *Nature* **615**, 111 (2023).
- <sup>15</sup>K. Schulten, C. E. Swenberg, and A. Weller, "A biomagnetic sensory mechanism based on magnetic field modulated coherent electron spin motion," *Z. Phys. Chem.* **111**, 1 (1978).
- <sup>16</sup>T. Ritz, S. Adem, and K. Schulten, "A model for photoreceptor-based magnetoreception in birds," *Biophys. J.* **78**, 707 (2000).
- <sup>17</sup>P. J. Hore and H. Mouritsen, "The radical-pair mechanism of magnetoreception," *Annu. Rev. Biophys.* **45**, 299 (2016).
- <sup>18</sup>N. Ozturk, C. P. Selby, S. H. Song, R. Ye, C. Tan, Y. T. Kao, D. P. Zhong, and A. Sancar, "Comparative photochemistry of animal type 1 and type 4 cryptochromes," *Biochemistry* **48**, 8585 (2009).
- <sup>19</sup>B. D. Zoltowski, Y. Chelliah, A. Wickramaratne, L. Jarocho, N. Karki, W. Xu, H. Mouritsen, P. J. Hore, R. E. Hibbs, C. B. Green, and J. S. Takahashi, "Chemical and structural analysis of a photoactive vertebrate cryptochrome from pigeon," *Proc. Natl. Acad. Sci. U. S. A.* **116**, 19449 (2019).
- <sup>20</sup>A. Günther, A. Einwich, E. Sjulstok, R. Feederle, P. Bolte, K.-W. Koch, I. A. Solov'yov, and H. Mouritsen, "Double-cone localization and seasonal expression pattern suggest a role in magnetoreception for European robin cryptochrome 4," *Curr. Biol.* **28**, 211 (2018).
- <sup>21</sup>T. Hochstoeger, T. Al Said, D. Maestre, F. Walter, A. Vilceanu, M. Pedron, T. D. Cushion, W. Snider, S. Nimpf, G. C. Nordmann, L. Landler, N. Edelman, L. Kruppa, G. Durnberger, K. Mechtler, S. Schuechner, E. Ogris, E. P. Malkemper, S. Weber, E. Schleicher, and D. A. Keays, "The biophysical, molecular, and anatomical landscape of pigeon CRY4: A candidate light-based quantum magnetosensor," *Sci. Adv.* **6**, eabb9110 (2020).
- <sup>22</sup>J. Xu, L. E. Jarocho, T. Zollitsch, M. Konowalczyk, K. B. Henbest, S. Richert, M. J. Goleworthy, J. Schmidt, V. Déjean, D. J. C. Sowood, M. Bassetto, J. Luo, J. R. Walton, J. Fleming, Y. Wei, T. L. Pitcher, G. Moise, M. Herrmann, H. Yin, H. Wu, R. Bartölke, S. J. Käsehagen, S. Horst, G. Dautaj, P. D. F. Murton, A. S. Gehrckens, Y. Chelliah, J. S. Takahashi, K.-W. Koch, S. Weber, I. A. Solov'yov, C. Xie, S. R. Mackenzie, C. R. Timmel, H. Mouritsen, and P. J. Hore, "Magnetic sensitivity of cryptochrome 4 from a migratory songbird," *Nature* **594**, 535 (2021).
- <sup>23</sup>P. Bolte, A. Einwich, P. K. Seth, R. Chetverikova, D. Heyers, I. Wojahn, U. Janssen-Bienhold, R. Feederle, P. J. Hore, K. Dedek, and H. Mouritsen, "Cryptochrome 1a localisation in light- and dark-adapted retinæ of several migratory and non-migratory bird species: No signs of light-dependent activation," *Ethol. Ecol. Evol.* **33**, 248 (2021).
- <sup>24</sup>D. R. Kattvig, I. A. Solov'yov, and P. J. Hore, "Electron spin relaxation in cryptochrome-based magnetoreception," *Phys. Chem. Chem. Phys.* **18**, 12443 (2016).
- <sup>25</sup>D. R. Kattvig, J. K. Sowa, I. A. Solov'yov, and P. J. Hore, "Electron spin relaxation can enhance the performance of a cryptochrome-based magnetic compass sensor," *New J. Phys.* **18**, 063007 (2016).
- <sup>26</sup>S. Worster, D. R. Kattvig, and P. J. Hore, "Spin relaxation of radicals in cryptochrome and its role in avian magnetoreception," *J. Chem. Phys.* **145**, 035104 (2016).
- <sup>27</sup>D. Kobylkov, J. Wynn, M. Winklhofer, R. Chetverikova, J. J. Xu, H. Hiscock, P. J. Hore, and H. Mouritsen, "Electromagnetic 0.1–100 kHz noise does not disrupt orientation in a night-migrating songbird implying a spin coherence lifetime of less than 10 μs," *J. R. Soc. Interface* **16**, 20190716 (2019).
- <sup>28</sup>H. Wu, A. Scholten, A. Einwich, H. Mouritsen, and K.-W. Koch, "Protein-protein interaction of the putative magnetoreceptor cryptochrome 4 expressed in the avian retina," *Sci. Rep.* **10**, 7364 (2020).
- <sup>29</sup>K. Görtemaker, C. Yee, R. Bartölke, H. Behrmann, J. O. Vofß, J. Schmidt, J. J. Xu, V. Solovyeva, B. Leberecht, E. Behrmann, H. Mouritsen, and K. W. Koch, "Direct interaction of avian cryptochrome 4 with a cone specific G-protein," *Cells* **11**, 2043 (2022).
- <sup>30</sup>K. Maeda, K. B. Henbest, F. Cintolesi, I. Kuprov, C. T. Rodgers, P. A. Liddell, D. Gust, C. R. Timmel, and P. J. Hore, "Chemical compass model of avian magnetoreception," *Nature* **453**, 387 (2008).
- <sup>31</sup>C. Kerpel, S. Richert, J. G. Storey, S. Pillai, P. A. Liddell, D. Gust, S. R. Mackenzie, P. J. Hore, and C. R. Timmel, "Chemical compass behaviour at microtesla magnetic fields strengthens the radical pair hypothesis of avian magnetoreception," *Nat. Commun.* **10**, 3707 (2019).
- <sup>32</sup>A. Weller, F. Nolting, and H. Staerk, "A quantitative interpretation of the magnetic field effect on hyperfine-coupling-induced triplet formation from radical ion pairs," *Chem. Phys. Lett.* **96**, 24 (1983).
- <sup>33</sup>K. Maeda, A. J. Robinson, K. B. Henbest, H. J. Hogben, T. Biskup, M. Ahmad, E. Schleicher, S. Weber, C. R. Timmel, and P. J. Hore, "Magnetically sensitive light-induced reactions in cryptochrome are consistent with its proposed role as a magnetoreceptor," *Proc. Natl. Acad. Sci. U. S. A.* **109**, 4774 (2012).
- <sup>34</sup>S. Y. Wong, P. Benjamin, and P. J. Hore, "Magnetic field effects on radical pair reactions: Estimation of  $B_{1/2}$  for flavin-tryptophan radical pairs in cryptochromes," *Phys. Chem. Chem. Phys.* **25**, 975 (2023).
- <sup>35</sup>S. Y. Wong, Y. Wei, H. Mouritsen, I. A. Solov'yov, and P. J. Hore, "Cryptochrome magnetoreception: Four tryptophans could be better than three," *J. R. Soc. Interface* **18**, 20210601 (2021).
- <sup>36</sup>M. D. Wheeler, S. M. Newman, A. J. Orr-Ewing, and M. N. R. Ashfold, "Cavity ring-down spectroscopy," *J. Chem. Soc., Faraday Trans.* **94**, 337 (1998).
- <sup>37</sup>G. Berden, R. Peeters, and G. Meijer, "Cavity ring-down spectroscopy: Experimental schemes and applications," *Int. Rev. Phys. Chem.* **19**, 565 (2000).
- <sup>38</sup>J. P. Norton, *An Introduction to Identification* (Academic Press, San Diego, CA, 1986).
- <sup>39</sup>A. van den Bos, *Handbook of Measurement Science*, edited by P. H. Sydenham (Wiley, NY, 1982).
- <sup>40</sup>A. A. Lee, J. C. S. Lau, H. J. Hogben, T. Biskup, D. R. Kattvig, and P. J. Hore, "Alternative radical pairs for cryptochrome-based magnetoreception," *J. R. Soc. Interface* **11**, 20131063 (2014).
- <sup>41</sup>K. Schulten and P. G. Wolynes, "Semiclassical description of electron spin motion in radicals including the effect of electron hopping," *J. Chem. Phys.* **68**, 3292 (1978).
- <sup>42</sup>C. R. Timmel, U. Till, B. Brocklehurst, K. A. McLauchlan, and P. J. Hore, "Effects of weak magnetic fields on free radical recombination reactions," *Mol. Phys.* **95**, 71 (1998).
- <sup>43</sup>A. I. Shushin, "The effect of the spin exchange interaction on SNP and RYDMR spectra of geminate radical pairs," *Chem. Phys. Lett.* **181**, 274 (1991).
- <sup>44</sup>K. Maeda, T. Miura, and T. Arai, "A practical simulation and a novel insight to the magnetic field effect on a radical pair in a micelle," *Mol. Phys.* **104**, 1779–1788 (2006).

<sup>45</sup>T. Miura, K. Maeda, and T. Arai, "The spin mixing process of a radical pair in low magnetic field observed by transient absorption detected nanosecond pulsed magnetic field effect," *J. Phys. Chem. A* **110**, 4151 (2006).

<sup>46</sup>O. Efimova and P. J. Hore, "Role of exchange and dipolar interactions in the radical pair model of the avian magnetic compass," *Biophys. J.* **94**, 1565 (2008).

<sup>47</sup>R. Haberkorn, M. E. Michel-Beyerle, and R. A. Marcus, "On spin-exchange and electron-transfer rates in bacterial photosynthesis," *Proc. Natl. Acad. Sci. U. S. A.* **76**, 4185 (1979).

<sup>48</sup>A. Ogrodnik, H. W. Kruger, H. Orthuber, R. Haberkorn, M. E. Michel-Beyerle, and H. Scheer, "Recombination dynamics in bacterial photosynthetic reaction centers," *Biophys. J.* **39**, 91 (1982).